CAT-ACT—A new highly versatile x-ray spectroscopy beamline for catalysis and radionuclide science at the KIT synchrotron light facility ANKA

A. Zimina, K. Dardenne, M. A. Denecke, D. E. Doronkin, E. Huttel, H. Lichtenberg, S. Mangold, T. Pruessmann, J. Rothe, Th. Spangenberg, R. Steininger, T. Vitova, H. Geckeis, and J.-D. Grunwaldt

Citation: Review of Scientific Instruments **88**, 113113 (2017);
View online: https://doi.org/10.1063/1.4999928
View Table of Contents: http://aip.scitation.org/toc/rsi/88/11
Published by the American Institute of Physics

CAT-ACT—A new highly versatile x-ray spectroscopy beamline for catalysis and radionuclide science at the KIT synchrotron light facility ANKA

A. Zimina,[1,2,a)] K. Dardenne,[3] M. A. Denecke,[4] D. E. Doronkin,[1,2] E. Huttel,[5] H. Lichtenberg,[1,2] S. Mangold,[6] T. Pruessmann,[1,2] J. Rothe,[3] Th. Spangenberg,[5] R. Steininger,[6] T. Vitova,[3] H. Geckeis,[3] and J.-D. Grunwaldt[1,2]

[1]*Institute of Catalysis Research and Technology (IKFT), Karlsruhe Institute of Technology, Eggenstein-Leopoldshafen, Germany*

[2]*Institute for Chemical Technology and Polymer Chemistry (ITCP), Karlsruhe Institute of Technology, Karlsruhe, Germany*

[3]*Institute for Nuclear Waste Disposal (INE), Karlsruhe Institute of Technology, Eggenstein-Leopoldshafen, Germany*

[4]*The University of Manchester, Dalton Nuclear Institute, Manchester, United Kingdom*

[5]*Institute for Beam Physics and Technology (IBPT), Karlsruhe Institute of Technology, Eggenstein-Leopoldshafen, Germany*

[6]*Institute for Photon Science and Synchrotron Radiation (IPS), Karlsruhe Institute of Technology, Eggenstein-Leopoldshafen, Germany*

(Received 11 August 2017; accepted 4 November 2017; published online 29 November 2017)

CAT-ACT—the hard X-ray beamline for CATalysis and ACTinide/radionuclide research at the KIT synchrotron radiation facility ANKA—is dedicated to X-ray spectroscopy, including "flux hungry" photon-in/photon-out and correlative techniques and combines state-of-the-art optics with a unique infrastructure for radionuclide and catalysis research. Measurements can be performed at photon energies varying between 3.4 keV and 55 keV, thus encompassing the actinide M- and L-edge or potassium K-edge up to the K-edges of the lanthanide series such as cerium. Well-established X-ray absorption fine structure spectroscopy in transmission and fluorescence detection modes is available in combination with high energy-resolution X-ray emission spectroscopy or X-ray diffraction techniques. The modular beamline design with two alternately operated in-line experimental stations enables sufficient flexibility to adapt sample environments and detection systems to many scientific challenges. The ACT experimental station focuses on various aspects of nuclear waste disposal within the mission of the Helmholtz association to contribute to the solution of one of the greatest scientific and social challenges of our time—the safe disposal of heat producing, highly radioactive waste forms from nuclear energy production. It augments present capabilities at the INE-Beamline by increasing the flux and extending the energy range into the hard X-ray regime. The CAT experimental station focuses on catalytic materials, e.g., for energy-related and exhaust gas catalysis. Characterization of catalytically active materials under realistic reaction conditions and the development of *in situ* and *operando* cells for sample environments close to industrial reactors are essential aspects at CAT. *Published by AIP Publishing.* https://doi.org/10.1063/1.4999928

NOMENCLATURE

ANKA	ÅNgstrøm source KArlsruhe
BPM	Beam position monitor
BPSS	Beamline personnel safety system
CAT-ACT	X-ray beamline at ANKA for CATalysis and ACTinide (radionuclide) research
CRG	Collaborative research group
CVD	Chemical vapor deposition
DCM	Double crystal X-ray monochromator
DRIFTS	Diffuse reflectance infrared fourier transform spectroscopy
ESRF	European Synchrotron Radiation Facility
EXAFS	Extended X-ray absorption fine structure
HAW	Highly radioactive nuclear waste
HEPA	High efficiency particulate filters
HGF	Helmholtz Association of German Research Centers
HRXES	High resolution X-ray emission spectroscopy
IBPT	KIT Institute for Beam Physics and Technology
IKFT	KIT Institute of Catalysis Research and Technology
INE	KIT Institute for Nuclear Waste Disposal
IPS	KIT Institute for Photon Science and Synchrotron Radiation
IR	infrared spectroscopy
ITCP	KIT Institute for Chemical Technology and Polymer Chemistry
KIT	Karlsruhe Institute of Technology
LURE	Laboratoire d'Utilisation du Rayonnement Électromagnétique (Orsay, France)
MARS	Multi-analyses on radioactive samples at SOLEIL
PLC	Programmable logic controller
PSI	Paul Scherrer Institute

a)Author to whom correspondence should be addressed: anna.zimina@kit.edu

ROBL	beamline of the Helmholtz-Zentrum Dresden Rossendorf at the ESRF
ROI	Region of interest
SCADA	Supervisory control and data acquisition
SLS	Swiss Light Source
SNF	Spent nuclear fuel
SOLEIL	Source Optimisée de Lumière d'Energie Intermédiaire du LURE
SR	Synchrotron radiation
XAFS	X-ray absorption fine structure
XANES	X-ray absorption near edge structure
XAS	X-ray absorption spectroscopy
XRD	X-ray diffraction
XRF	X-ray fluorescence analysis

I. INTRODUCTION

X-ray absorption spectroscopy and emission spectroscopy are key techniques in a well-established toolbox in material science, solid state chemistry and physics, biology, and environmental and catalysis research because they are very powerful and, in some cases, unique methods to probe the local atomic structure of solids, liquids, and gases.[1,2] X-ray techniques allow probing the electronic structure of materials, following the bond formation, and studying charge transfer effects and magnetic behavior. The development of synchrotron radiation technology providing intense and tunable X-ray sources enhanced the use of these methods and initiated their continued improvement. Synchrotron radiation sources are steadily challenged by new requirements arising from advanced scientific questions and altered industrial demands. In addition, improved detection systems like highly sensitive semiconductor fluorescence detectors for low concentrated species, surface and reflection X-ray absorption spectroscopy (XAS) for probing thin films and adsorbents, and dispersive and time resolved setups for kinetic studies are developed. Nevertheless, the existing experimental setups all over the world still do not fully cover the demand in all application areas, like radionuclide and catalyst research. Moreover, due to the specific requirements to sample environments and sample treatment protocols, combined experiments for these research areas require optimized procedures at synchrotron radiation sources.

As a result of nuclear energy use over decades, a final volume of 29.000 m^3 heat generating highly radioactive waste [HAW: spent nuclear fuel (SNF) and highly active waste from fuel reprocessing] will be generated until phase out of nuclear power generation in Germany in 2022.[3] Additionally, a total amount of about 300.000 m^3 of radioactive waste with negligible heat generation already exists or will result from ongoing scientific, medical, or technological applications—including activated debris from the decommissioning of nuclear power plants.[4] Internationally, final disposal in deep bedrock repositories is deemed as the preferred option for the management of low, intermediate (i.e., not heat producing), and high level nuclear waste (SNF and vitrified residues from fuel reprocessing). In the German context, a dedicated separate repository for the heat producing HAW fraction is conceived. Solving the nuclear disposal safety case requires the assessment of an envisaged disposal site on geological time scales, where speciation techniques like X-ray absorption fine structure (XAFS) spectroscopy provide necessary input parameters to model long-term geochemical behavior and reactive transport phenomena of radiotoxic nuclides [i.e., uranium and *trans*-uranium actinide (An) elements generated during reactor operation as well as long-lived fission and activation products].[5,6] Various processes determining radionuclide mobilization and/or retention following their hypothetical release from a bedrock repository site (e.g., as a consequence of groundwater intrusion and mechanical or corrosive degradation of technical barriers, containments, and HAW matrices) have been identified or elucidated based on XAFS studies, e.g., formation of water soluble complexes or colloids under various solubility determining boundary conditions (e.g., pH, eh, ionic strength, and temperature), transport with groundwater advection in fractured/porous host rock formations, diffusion along concentration gradients (e.g., in claystone backfill of buffer materials), surface sorption, and precipitation or radionuclide incorporation into secondary phases forming during corrosion of disposal containers and technical barriers (e.g., backfill materials and concrete liners of emplacement galleries). More recently, additional attempts to directly characterize HAW matrices by XAFS techniques were brought into focus by several groups, mainly due to the necessity to assess effects of an extended interim storage period above or near surface preceding deep geological disposal, such as embrittlement of fuel pin claddings.[7–9] Although standard X-ray absorption spectroscopy and advanced high resolution X-ray emission spectroscopy techniques possess high potential to elucidate the chemical state and electronic structure of radionuclides in various matrices—a prerequisite for predicting their reactivity and long-term environmental impact[7,10–15]—synchrotron based facilities for such investigations are sparsely available. In Europe, these are (in the order of their commissioning) the Rossendorf Collaborative Reasearch Group (CRG) beamline (BM20 ROBL) at the ESRF in Grenoble (France),[16] the INE-Beamline for radionuclide science at KIT-ANKA in Karlsruhe (Germany),[17] the μ-XAS beamline at PSI-SLS in Villigen (Switzerland),[18] and the MARS beamline at SOLEIL in Gif-sur-Yvette (France).[19]

For catalysis research, *in situ* and *operando* X-ray based characterization methods have emerged as key techniques for a rational design of heterogeneous catalysts.[20–25] This approach was not only appreciated by the scientific community, but also applied by industry, such as Haldor Topsøe A/S, Exxon, UOP, IFP, or Umicore. Knowledge of oxidation state, coordination environment, and nanoparticle morphology contributed significantly to a deeper understanding of heterogeneously catalyzed reactions and serves today as a basis for the design of new catalysts and for first-principles kinetic modeling.[1,26] Strong cooperation between academic research and industry stimulated the improvement of catalytic materials in various applications.[20,23,24] One of the most prominent examples is the development of exhaust gas after-treatment systems. Main pollutants in diesel, Otto, and lean-burn engines' exhaust gases are NO_x, CO, hydrocarbons, and soot particles.[27,28] Successful efforts were undertaken to improve the performance of the classical three-way-catalysts (TWC) for gasoline engines and

selective catalytic reduction and NO_x storage-reduction (NSR) catalysts for diesel engines applying the "knowledge-based-design" concept. Nevertheless, various challenges remain, mainly with respect to poisoning and thermal deterioration. Other important applications are methanol synthesis[29,30] and Fischer-Tropsch synthesis,[31] i.e., commercialized technologies for converting synthesis gas (a mixture of CO and H_2) into fuels and chemicals. This pathway has great potential for producing synthetic fuels from renewable sources, such as biomass[32] after its thermochemical conversion into synthesis gas or from solar or wind energy via hydrogen,[33,34] and requires highly efficient catalysts.

The importance of studying catalysts under realistic reaction conditions was demonstrated previously.[20,22,23,35] For example, structural changes in a Pt–Rh catalyst for the partial oxidation of methane were monitored while exposing the metal particles to a $6\%CH_4/3\%O_2$/He gas mixture and varying the temperature (heating up to 500 °C followed by cooling down to room temperature). Reduction at 330 °C followed by re-oxidation during cooling was observed, a process which would stay undiscovered in the case of *ex situ* measurements.[36] Another example for the importance of *in situ* studies is the total oxidation of methane over a Pd/ZrO_2 catalyst.[37,38] The catalytic activity is high up to 700 °C but decreases above that temperature. *In situ* XAS and XRD measurements showed that the reason for this behavior is the formation of metallic Pd particles and their sintering at elevated temperatures. Another illustrative case study is the hydrogenation of CO/CO_2 over copper particles where EXAFS and XRD data revealed a strong influence of the reaction conditions on the morphology and microstructure of the catalyst.[30,39]

There are several synchrotron light sources in Europe with beamlines dedicated to *in situ* and *operando* XAS studies, e.g., ID24[40] and BM31[41] at ESRF in Grenoble (France), ROCK at SOLEIL near Paris (France),[42] ANKA-XAS in Karlsruhe (Germany),[43,44] and SuperXAS at PSI-SLS in Villigen (Switzerland)[45] as well as the recently established P64[46] and P65[47] lines at PETRA III (succeeding X1 at the old DORIS storage ring at DESY) in Hamburg (Germany) and Balder at MAX IV in Lund (Sweden).[48] However, the growing demand for specific infrastructure for spectroscopic studies on catalytic materials is still not fully covered, especially if catalytic engineering is to be brought together with spectroscopy.

This publication describes the layout of the newly established CAT-ACT beamline at the KIT synchrotron radiation facility (ANKA) and its experimental infrastructure embedded into the KIT lab environment. In Sec. VII, examples for recent and ongoing research projects conducted at CAT-ACT are presented. These specific examples have been selected to demonstrate the advantages offered by the CAT-ACT beamline to the catalysis and radionuclide communities: close proximity to well-equipped laboratories, a broad range of available energies, and variability in its modular design. An outlook on future opportunities and possibilities for beamtime access at ANKA is presented at the end.

II. THE KIT SYNCHROTRON RADIATION FACILITY (ANKA)

KIT-IBPT operates the 110 m circumference storage ring ANKA as a test facility for accelerator development and SR

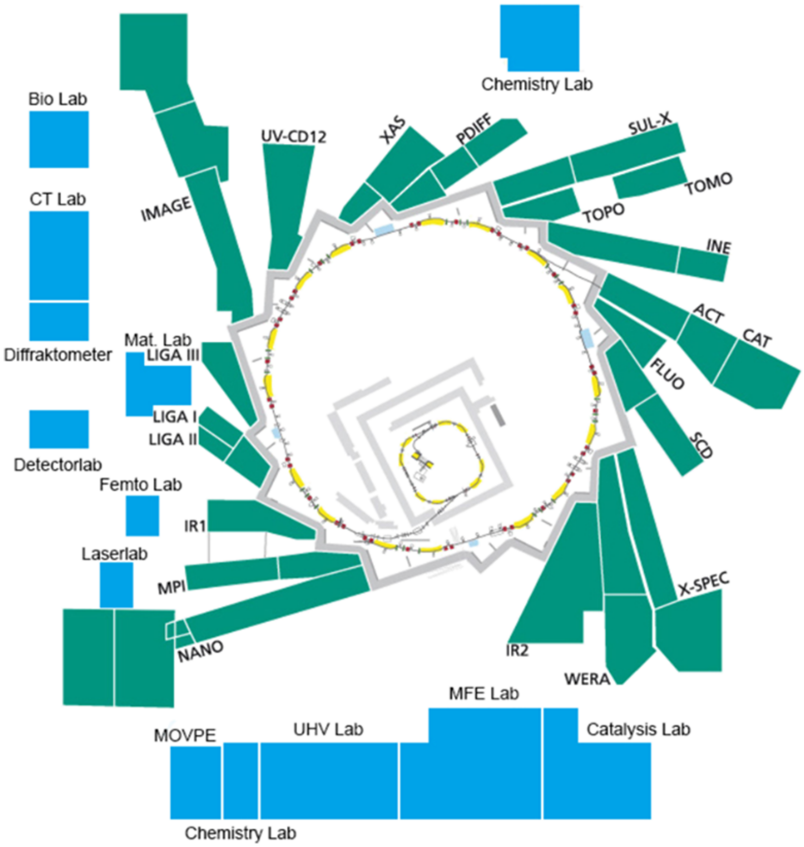

FIG. 1. Layout of the ANKA accelerator and storage ring complex with beamlines (marked in green) and auxiliary laboratories (marked in blue). The CAT-ACT beamline with its optics hutch and two in-line experimental end stations is located in the eastern part of the ANKA hall.

technologies and as synchrotron light source for KIT and HGF internal research programs. The ANKA accelerator complex (Fig. 1) consists of a 53 MeV microtron as a pre-accelerator, a 500 MeV booster synchrotron, and a 2.5 GeV electron storage ring. The injector has a repetition rate of 1 Hz and the booster current is about 5 mA. In standard SR operation, injection into the storage ring takes place two times a day with a nominal current of up to 200 mA accumulated in the storage ring at an electron energy of 500 MeV which is then ramped up to 2.5 GeV. For 150 mA, the lifetime of the stored beam at 2.5 GeV is about 16 h. ANKA provides an electromagnetic spectrum ranging from the terahertz (THz) region to hard X-rays (the critical energy of the bending magnet spectrum is at 6 keV) for use in basic research and technological applications including micro- and nano-fabrication.[49] ANKA offers several operation modes, with a main distinction between standard operation at 2.5 GeV and lower energies of stored electrons—e.g., a low alpha mode at 1.3 GeV for generation of ultra-short electron bunches for coherent THz radiation. The storage ring parameters are summarized in Table I. Analytical science and micro-fabrication work at ANKA is embedded in a unique research environment. Besides performing SR experiments at the different beamline end stations (e.g., for XAS, XRD, XRF, X-ray tomography, UV-vis circular dichroism, and IR spectroscopy), experimenters at ANKA can potentially use a specialized laboratory infrastructure available at different nearby KIT institutes for sample preparation and/or characterization offering a variety of sophisticated laboratory techniques. Examples for synergistic utilization of synchrotron based and laboratory methods are the INE-Beamline[17] in combination with INE's on-site controlled area laboratories and the Karlsruhe Nano and Micro Facility (KNMF[50]). This successful concept will be adhered to in the near future by implementing the ANKA Lab for Catalysis Research in cooperation with IKFT and ITCP.

TABLE I. ANKA storage ring and CAT-ACT superconducting wiggler parameters.

Circumference	110.4 m
Number of long straight sections	4
Critical photon energy (bending magnet)	6 keV
Injection energy	0.5 GeV
End energy	2.5 GeV
Nominal electron current	200 mA
Radio frequency (RF)	500 MHz
Horizontal emittance	50 mrad
Horizontal beta-function, min–max	0.8–15 m
Vertical beta-function, min–max	1.7–30 m
CAT-ACT wiggler source	
Field strength	2.5 T
K	11.2
Vacuum gap	15 mm
Critical photon energy	10.2 keV
Total radiated power	4.7 kW
Horizontal beam size/divergence	0.3/0.19 mm/mrad
Vertical beam size/divergence	0.1/0.01 mm/mrad
Horizontal fan accepted by the front end aperture	1.5 mrad

III. THE CAT-ACT BEAMLINE AT ANKA

"CAT-ACT," a new highly versatile, high-flux hard X-ray beamline for CATalysis and ACTinide/radionuclide research, was recently installed at the synchrotron facility ANKA at KIT. The beamline was successfully commissioned in 2016 and is jointly operated by research groups at the Institute for Chemical Technology and Polymer Chemistry (ITCP, KIT), the Institute of Catalysis Research and Technology (IKFT, KIT), and the Institute for Nuclear Waste Disposal (INE, KIT), which have essential expertise in the two main application fields. The beamline optic design was developed and realized in close collaboration with scientists from the Institute for Beam Physics and Technology (IBPT, KIT) and the Institute for Photon Science and Synchrotron Radiation (IPS, KIT). CAT-ACT helps serve the growing need for high flux/high energy X-ray spectroscopy, complementing strongly overbooked existing beamlines in the fields of catalysis and radionuclide research.

The beamline design places emphasis on XAS in terms of X-ray absorption near edge structure (XANES) and extended X-ray absorption fine structure (EXAFS) combined with "flux hungry" photon-in/photon-out techniques such as HRXES. CAT-ACT comprises two alternately usable in-line experimental end stations: ACT for radionuclide research and CAT for catalytic studies. ACT is equipped with a specialized infrastructure and provides sophisticated containment concepts for experiments with highly radioactive samples. Correlative methods such as XAS in combination with X-ray diffraction (XRD), X-ray fluorescence analysis (XRF), and further photon spectroscopies (infrared, UV-vis) are provided at both experimental stations—with additional gas analysis (mass spectrometry and gas chromatography) for *in situ* and *operando* catalytic studies under relevant conditions (pressure and temperature) at CAT.

A. Layout and characteristics

In 2011, the ANKA experimental hall was extended at its east side to accommodate the CAT-ACT radiation protection hutches and the control cabin. The beamline comprises four sections—the optics hutch attached to the storage ring radiation protection wall, the ACT hutch with an adjacent personnel lock providing access control to the experimental station, the CAT hutch, and a separated control cabin. The beamline layout and schematic beam path are depicted in Fig. 2.

To increase the available photon flux in order to fully exploit the potential of advanced X-ray emission/inelastic X-ray scattering spectroscopy, in order to overcome the lower detection limits for investigations of dilute sample systems, and to extend the energy range for XAS studies into the hard X-ray regime, a superconducting 2.5 T multipole wiggler source—designed and built by Budker Institute of Nuclear Physics (Novosibirsk, Russia)—was installed in summer 2014 in a short straight section opposite from the injection septum of the storage ring. The major wiggler parameters are listed in Table I. This insertion device provides access to K absorption edges of heavy elements like Rh, Pd, Ag, and Ce (of particular interest for catalysis research), and actinide L_1-edges and lanthanide K-edges up to Dy, while the low energy limit of the beamline still allows investigations at the K-edges of the

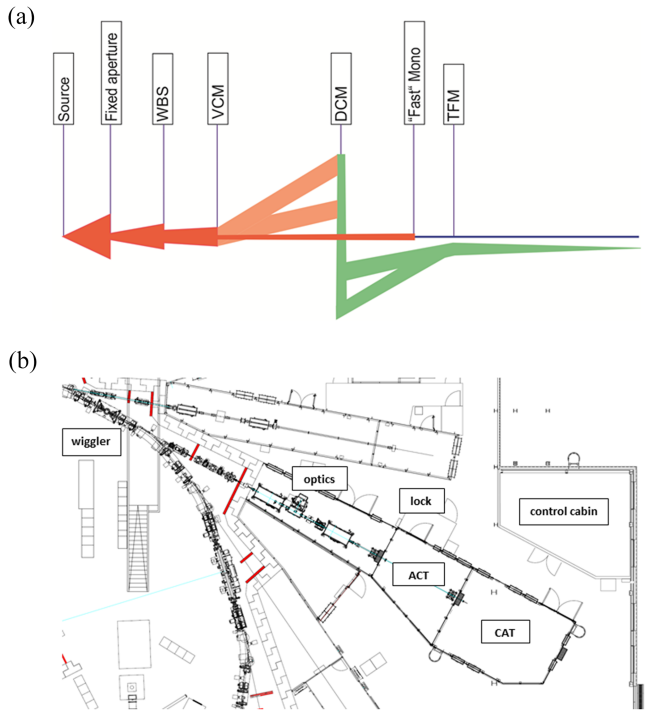

FIG. 2. (a) Schematic beam path (not to scale) from the source (left) to the experiments (right), visualizing the arrangement of the major CAT-ACT optical components: WBS—white beam slits, VCM—vertically collimating mirror, DCM—double crystal monochromator, TFM—toroidal focusing mirror, "Fast" Mono—the possible position for future insertion of a fast Quick-XAS DCM; (b) layout of the CAT-ACT facility with the optical hutch adjacent to the storage ring wall, two in-line experimental stations, and separate control cabin in the ANKA east hall extension.

early transition metals and actinide $M_{4,5}$-edges. The available photon flux at 20 keV is about two orders of magnitude higher compared to ANKA bending magnet radiation, which is especially beneficial with respect to the spectroscopic sensitivity for dilute sample systems, e.g., for studying catalyst promoters and poisons or trace concentrations in environmental radionuclide studies.

The wiggler beam is extracted from the zero degree port 3.3-0 at the storage ring dipole chamber adjacent to the straight section hosting the source. The beamline front end inside the radiation protection wall was designed, built, and installed in 2014 by FMB Berlin (Berlin, Germany). It consists of—in the order from the beam port to the wall tube—an X-ray beam position monitor (BPM), an intensity absorber, a total power limiting aperture [1.5 (h) × 0.67 (v) $mrad^2$], a vacuum protection shutter, a horizontal and vertical white beam slit assembly, and radiation protection shutter 1 (separating the front end and optic section). The beamline optics were designed, manufactured, and installed in the optics hutch in the first half of 2015 by FMB Oxford (Oxford, United Kingdom). Figure 3 depicts the main beamline optical components in the downstream order from the storage ring wall: an upward reflecting vertically collimating mirror (M1), a double crystal monochromator (DCM), a beam diagnostic unit (profile monitors, fluorescence screen, and white beam stop), and a downward reflecting toroidal focusing mirror (M2). M1 (flat, dynamic tangential bender) comprises three zones on a single Si substrate: pure Si, a Rh coated stripe, and a Pt coated stripe. This mirror acts as a collimator and low pass filter for rejection of higher harmonic radiation. M2 comprises two independent substrates with (M2-A) an axial bare Si cylinder on a dynamic tangential bender for horizontal and vertical (toroidal) focusing

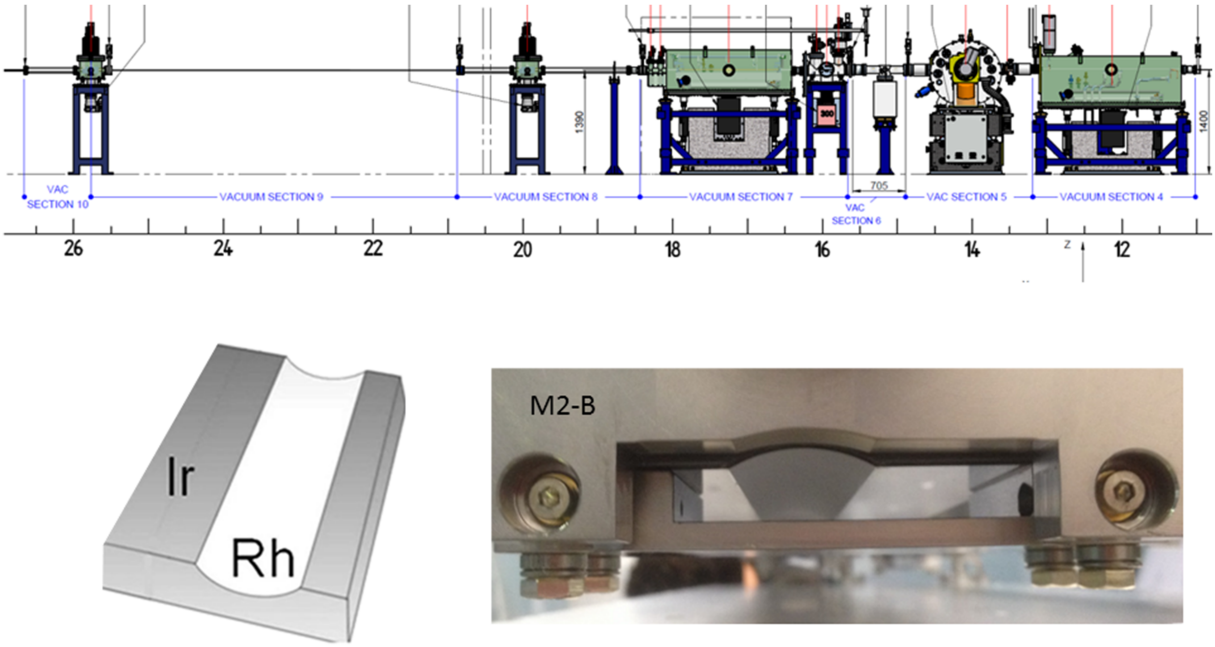

FIG. 3. (Top) CAD drawing of main CAT-ACT optical components. From right to left: M1, DCM, ion pump stand (to be replaced by fast Quick-XAS DCM in a future beamline upgrade), diagnostic module, M2, radiation protection shutter 2 (separating optic and ACT station), radiation protection shutter 3 (separating ACT and CAT stations). The scale at the bottom marks the distance in m from the wiggler source; (bottom left) schematic arrangement of M2-B reflecting zones; (bottom right) original photography of the M2-B substrate comprising a Rh-coated trough (left-hand side) and an Ir-coated flat zone (right-hand side).

and (M2-B) an axial Rh coated cylinder with an adjacent flat Ir coated zone on a common dynamic tangential bender for toroidal (Rh) or vertical (Ir) focusing, respectively (see Fig. 3). In the DCM pairs of Si(111) and Si(311), crystals are installed on a common Bragg-axis. A specific crystal pair is selected by motorized lateral translation of the DCM vacuum vessel. Both sets of crystals are liquid nitrogen cryo-cooled. The heat load introduced by the CAT-ACT wiggler leads to a (calculated) maximum absorbed power of 1250 W at M1, 314 W at the combined CVD filter/fluorescence screen inside the M1 vessel preceding the DCM and additional 700 W at the first DCM crystal. M1 and the CVD screen (a new FMB Oxford design withstanding the high heat load, comprising a 250 μm thick diamond window brazed to a thicker CVD diamond ring which in turn is brazed onto a short copper cylinder) are water cooled. Between the DCM and the diagnostic module, preceding M2 additional space is available for later insertion of a fast "Quick-EXAFS" DCM allowing higher XAFS scan repetition rates for studying dynamic processes.[51] The optical components are designed to deliver high monochromatic beam intensity (flux up to 10^{13} photons/s × 100 mA) in a wide photon energy range (3.4–35 keV with mirrors) at both experimental stations (focal spot in the ACT hutch at 22.8 m and in the CAT hutch at 28.05 m from the source, respectively). Parallel alignment of the DCM crystals at the rocking curve maximum may be detuned to achieve constant I_0 or I_0/I_{ring} flux conditions during energy scans (where I_0 denotes the intensity signal of the first ionization chamber at the individual experiments or—alternatively—the photocurrent delivered by a retractable tungsten mesh placed in the monochromatic beam downstream from the M2 vessel and I_{ring} denotes the storage ring current), applying a closed-loop feedback system (Mostab) developed by KIT-IPS based on a NI Compact RIO controller (National Instruments Germany GmbH, München).

The beam delivery system allows a closed beam path, i.e., fixed beam height 10 mm below the storage ring plane at both experiments for all mirror and DCM configurations. Mirrorless operation is possible above 35 keV. Using the toroidal mirror, the beam can be focused down to 1 × 1 mm^2 up to 35 keV at the CAT sample position and up to 27 keV at the ACT sample position. Above these energies, the beam size increases to about 2 × 1.5 mm^2. Examples for optic configurations covering various energy ranges at the two experimental stations, the corresponding mirror incidence angles, and further optical component parameters are listed in Table II. Focus size ("mirror operation") or beam foot print ("high energy operation") and the beam stability at the CAT and ACT sample positions are controlled by two "NanoBPM" devices (FMB Oxford patent) which can be installed at the individual sample stages. The two in-line experimental stations are used in an alternating fashion. To deliver beam to the CAT station, a segmented vacuum pipe can be easily inserted to bridge the ACT experiment.

A thorough beamline commissioning was performed in 2016 and the main characteristics proved to meet the original specifications. Figure 4 shows the photon flux as a function of photon energy, measured at the ACT experiment using a calibrated photodiode (HAMAMATSU Ltd.). The obvious discrepancy relative to the designed flux values is due to the actual necessity to operate the beamline at a reduced white beam slit aperture of 2 (h) × 1 (v) mm^2, reducing the total

TABLE II. CAT-ACT beamline optic parameters and examples for configurations covering various energy ranges at CAT and ACT experimental stations.

Energy range	3.4 keV–55 keV (wavelength range: 3.6–0.2254 Å)
Flux	At present time 10^{11} photons/s at 20 keV, Si(111), 100 mA
Source	2.5 T SC wiggler, (E_c = 10.2 keV)
Energy resolution	$E/\Delta E > 1 \times 10^4$
Beam spot size	Below 1 × 1 mm^2 up to 35 keV
Primary optics	Vertically collimating Si 1st mirror with bare Si/Rh/Pt coated stripes (bend radius 5 km < R < 40 km), fixed-exit DCM with LN_2 cooled crystals, and piezo-driven detuning/feedback system for the second crystal, direct drive Bragg axis goniometer with a maximum speed of 4° s^{-1} and exchangeable crystal pairs Si(111) and Si(311), focusing the 2nd mirror with the bare Si zone (bending radius 2.4 km < R < 10 km, 37 mm sagittal radius), Rh-coated zone (bending radius 2.4 km < R < 10 km, 25.2 mm sagittal radius), and Ir-coated zone (bending radius 2.4 km < R < 10 km, flat)

Station	Energy (keV)	VCM/M1	DCM	TFM/M2	Beam incidence (mrad)
ACT	4-7	Si stripe	Si(111)	Si cylinder	4.40
	7-10	Si stripe	Si(111)/Si(311)	Rh cylinder/Ir flat	3.00
	10-21	Rh stripe	Si(111)/Si(311)	Rh cylinder/Ir flat	3.00
	21-26	Pt stripe	Si(311)	Rh cylinder/Ir flat	3.00
	26-40	Pt stripe	Si(311)	Ir flat	1.90
	46-60	Out of beam	Si(311)	Out of beam	...
CAT	4-11	Si stripe	Si(111)	Si cylinder	2.78
	11-16.5	Si stripe	Si(111)	Rh cylinder/Ir flat	1.90
	16.5-22	Rh stripe	Si(111)/Si(311)	Rh cylinder/Ir flat	1.90
	22-45	Pt stripe	Si(311)	Rh cylinder/Ir flat	1.90
	45-55	Out of beam	Si(311)	Out of beam	...

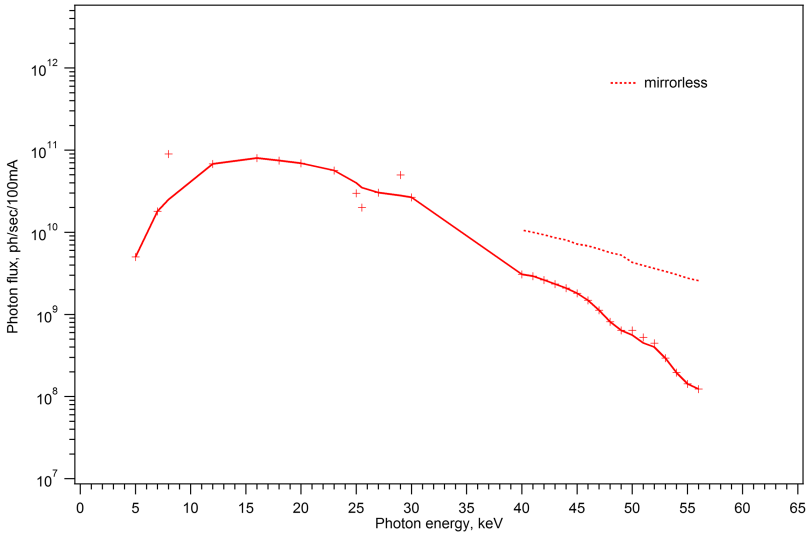

FIG. 4. Photon flux measured at the ACT experimental station using a calibrated photodiode placed at the focus position.

flux to less than 5% of the flux delivered to the experiments at a full acceptance angle. This precaution measure had to be imposed as the original water-cooled CVD diamond filter/screen located in the M1 vessel (serving as white/pink beam diagnostics and limiting the thermal load on the vacuum protection window at the DCM entrance flange) was initially damaged due to unexpectedly high wiggler beam heat load. This component has meanwhile been redesigned and replaced (cf. Sec. III A above), and its commissioning is ongoing. Figure 5 depicts a selection of XAS spectra recorded in different energy ranges using suitable optic configurations. The energy resolution as manifested by the steepness of the XANES rising edge (determined through the full width at half maximum width of the main feature of the first derivative, taking into account corresponding core level lifetime values) has been experimentally determined for the different energies and varies from 0.15 eV (BaTiO3, at the Ti K-edge, 4966 eV, natural core level width 0.67 eV) with DCM Si(111) to 2.10 eV (Mo metal at the Mo K-edge, 20 000 eV, natural core level width 4.52 eV) using DCM Si(311).

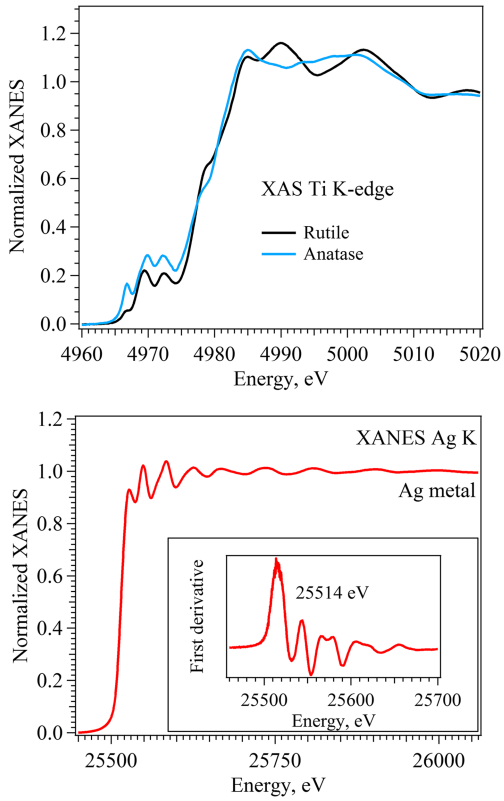

FIG. 5. Selected XAS spectra recorded during commissioning phase: (top) Ti K XANES of TiO_2 rutile and anatase phase; (bottom) Ag K XANES of the Ag foil and its first derivative.

Parallel to the commissioning of the beam delivery system, the core experimental infrastructure at the CAT and ACT end stations was set up and tested—cf. Secs. IV–VI. The beamline was successfully integrated into the ANKA personnel safety, vacuum, and radiation protection system and licensed for general user operation.

B. Control system

Complying to the standard at all ANKA beamlines, the CAT-ACT operation, safety, and control system rests on two pillars—the command line based experiment control software SPEC [Certified Scientific Software, Cambridge (MA), USA] handles all data acquisition and motor positioning tasks, while the beamline personnel safety system (BPSS) is based on a fail-safe PLC (Pilz GmbH, Ostfildern, Germany) in combination with a SIMATIC WinCC Open Architecture SCADA system (ETM professional control GmbH, Eisenstadt, Austria).[52] An additional TANGO layer[53] was introduced to control more complex data acquisition and motor devices.

A major challenge with respect to the implementation of the beamline control system was to allow for fast and reproducible switching between the 23 main configurations for optic adjustments necessary to deliver beam to the two different end stations at different energies, where each parameter set (mirror incident angle, reflecting zone, focusing trough, DCM height, crystal gap, etc.) defines conditions to optimize flux, energy resolution, higher harmonic content, beam spot size, etc. in a limited photon energy range. All relevant axes are equipped with position encoders. To be able to change between energy

ranges and experimental stations quickly, a SPEC macro based on a lookup table containing all possible positions of the optical elements was developed. Following the user input of a desired experimental station and energy range, the corresponding set of positions is selected by the macro. All motors are moved incrementally inside a loop until all target positions are reached. The motor temperatures are checked before each movement to make sure that the motors do not overheat. Motors reaching temperatures above 80 °C (mostly in-vacuum motors of mirror benders and horizontal translation) are skipped in the current loop until they have cooled down. As an additional safety feature, the first radiation protection shutter is closed at the beginning of the positioning procedure to ensure that no optical elements are driven through the white beam. The energy to the Bragg angle conversion is handled by SPEC while the additional motor positions necessary for the fixed exit mode (DCM height, 2nd crystal parallel and perpendicular positions) are calculated internally by the DCM controller [Omron Delta Tau UMAC, Chatsworth (CA), USA]. Communication between the SPEC user command layer and the DCM controller is passed through a TANGO server. The SPEC control system runs on a cluster of three Linux PCs, where the master optics PC shares access to user relevant motor positions and adjustments with two additional PCs for CAT and ACT experiment surveillance.

IV. EXPERIMENTAL METHODS AND INSTRUMENTATION

In Sections IV A and IV B, the experimental infrastructure available at the two alternately operated experimental end stations CAT and ACT is described.

A. ACT station (experiment 1)

After installation of a fixed height 2.1 × 1.4 m^2 optical breadboard table (Newport, France), the components of a Johann-type multi-analyzer crystal HRXES spectrometer with 1 m Rowland circle diameter (based on an original ESRF design[54,55])—which was previously commissioned and extensively used at the INE-Beamline[55–57]—were craned into the ACT hutch and precisely aligned to a permanent position relative to the X-ray focus inside the hutch (as defined by the toroidal second mirror of the CAT-ACT optic). The spectrometer assembly comprises a positioning stage with four degrees of freedom for each of the five spherically shaped analyzer crystals which focus fluorescence radiation in a narrow energy bandpass onto the detector. The detector positioning unit comprises three degrees of freedom (a crossed long and short linear stage and a rotation stage). The entire setup allows the crystals and the detector to be moved along the vertical Rowland circles intersecting at the sample surface and the detector [AXAS-M silicon drift detector (SDD, KETEK GmbH, Munich, Germany)] entrance window positions. This setup allows for high precision Bragg angle/emission energy scans. Depending on the analyzer crystal set [currently available: Si(111), Ge(111), Si(110)], Bragg angle, diffraction order, and beam spot size, an energy resolution of about 1.0 eV (Np M_5-edge) has been achieved (cf. Sec. VII A). The crystal and detector positioning system was supplemented by a 4-axis (x,y,z,φ) sample positioning stage and a two-axis positioning stage for auxiliary slits or pinholes in front of the sample (all from Huber Diffraktionstechnik, Rimsting, Germany). For standard XAFS data acquisition in transmission and total fluorescence yield detection mode, an optical bench based on X-95 profile rails holding three ionization chambers for simultaneous sample and reference sample measurements in transmission mode (Poikat, Hamburg, Germany) was installed. A 5-element LEGe solid state fluorescence detector (Canberra-Eurisys, Olen, Belgium)—previously as well operated at the INE-Beamline—was moved to the ACT station, as it permits detection of high energy photons up to the Kα lines of the early lanthanides that are now accessible. Although CAT-ACT with its 2.5 T superconducting wiggler source is optimized for hard X-ray operation, the achievable low energy limit of about 3.4 keV in the *tender* X-ray regime permits highly efficient absorption and emission spectroscopy at the An $M_{4,5}$-edges (the U M_4-edge, e.g., is at 3.73 keV). To avoid scattering and absorption in air, at these energies all beam paths at the ACT experiment can be kept in a pure He atmosphere by installation of a temporary gas tight structure consisting of a rigid plexiglass frame bolted to the experiment table, which spans two flexible bags surrounding the analyzer crystals and the detector. Those stay freely movable along their individual Rowland circles. All currently available detectors at the CAT-ACT beamline are listed in Table III. Fully digital data processing for fluorescence spectra (XRF, fluorescence yield XAS) acquisition is provided employing XMAP DXP modules controlled by the X-Manager software [XIA LLC, Hayward (CA), USA]. Region of interest (ROI) setting, fluorescence line integration, and read out are accomplished by a TANGO server based on the system developed by Mangold *et al.*[58] The current setup is depicted in Fig. 6.

B. CAT station (experiment 2)

The large 41 m^2 experimental hutch is dedicated to *in situ* and *operando* catalytic studies requiring sample environments as close as possible to realistic conditions (high temperature, elevated pressure, liquid/gas phase, etc.) together with the freedom to unite the diagnostic setups and complementary techniques at one place. The basic component of the CAT experimental station is a motorized kinematic optical positioning table carrying the setup for XAS measurements in transmission mode (Fig. 7). Three ionization chambers for nominally high energies (Ohyo Koken Kogyo, Co., Ltd., Japan), mounted in series on X-95 profiles along with the signal acquisition and processing chain consisting of Keithley 428 Electrometers (Tektronix UK Ltd., UK) and voltage-to-frequency converters (NOVA R&D, Inc., USA), provide high quality transmission signals in a wide range of photon energies. The gas filling of ionization chambers and the applied voltage can be set individually for each chamber to optimize the signal-to-noise ratio in different energy ranges. A large area PIN photodiode (HAMAMATSU Ltd., Japan) can be used for collecting total fluorescence XAS data, e.g., on non-transparent samples. A slit system of motorized high precision horizontal and vertical blades is installed in front of the first ionization

TABLE III. Experimental and sample environment at ACT and CAT stations.

ACT station:
• High precision HUBER (Huber Diffraktionstechnik, Rimsting, Germany) x,y,z,φ sample positioning system, two linear stages perpendicular and parallel to the beam axis (±40 mm, step size = 0.1 μm); z height adjustment (0–90 mm, step size = 50 nm); the 360° rotation stage (step size = 0.001°)
• 2.1 × 1.4 m^2 fixed height breadboard optical table
• Fully equipped and licensed to handle radionuclides in a double containment up to 1.0 × 10^6 times the exemption limit
• Sealed media feedthrough chicanes and separate ventilation/filter system for experimental hutches
• Access through personnel lock with a hand/foot contamination monitor
• Ionization chambers for nominally high energies (IONIKA DN160 ISO-K-L150 & -L200, HASYLAB Poikat design, RAPO engineering, Appen, Germany)
• I_0 ionization chamber for nominally low energies (<5 keV), Oken Ltd., Japan
• Current amplifier DLPCA-200 (FEMTO Messtechnik GmbH, Berlin, Germany) voltage-to-frequency converters (NOVA R&D, Inc., USA)
• 23-axis Johann type high resolution emission spectrometer (Huber Diffraktionstechnik, Rimsting, Germany) with five intersecting Rowland circles, analyzer crystal sets [Si(111), Ge(111), Si(110)] for actinide $M_{4,5}$- and L_3-edges—angular range available: 67°-88°
• 5-pixel low energy Ge solid state fluorescence detector (Canberra-Eurisys Ultra-LEGe, Olen, Belgium)
• AXAS-M silicon drift detector (SDD, KETEK GmbH, Munich, Germany)
• Fully digital fluorescence detector read-out (XIA DXP-xMAP, XIA LLC, Hayward, CA, USA)
CAT station:
• Auxiliary horizontal and vertical slit
• 1.2 × 3 m^2 breadboard optical 6-axis motorized kinematic table (load capacity 500 kg)
• Ionization chambers for nominally high energies (Ohyo Koken Kogyo Co. Ltd., Japan)
• Keithley 428 electrometers (Tektronix UK Ltd., UK)
• Large area PIN photodiode (HAMAMATSU Ltd., Japan)
• MediPix area detector: active area: 42.6 × 28.4 mm^2, pixel pitch: 55 μm, sensor material Si: 500 μm, frame rate: 6.5 fps/8.8 fps burst mode (University of Freiburg, Germany)
• High precision/heavy load hexapod sample positioning system (Physik Instrumente, Model H-850), maximum load 250 kg
• Independent ventilation and chemical exhaust system
• On-site reactive gas supply
• Mobile gas dosing unit with integrated mass flow controllers (Bronkhorst High-Tech B.V., Germany)
• Mass spectrometer (ThermoStar™ GSD 320, Pfeiffer vacuum)
• Gas blower, heating up to 900 °C (FMB Oxford, UK)
• Continues flow quartz capillary setup

chamber, providing the opportunity to define the beam size according to the selected sample configuration. A heavy duty hexapod H-850 with a load capacity up to 250 kg (Physik Instrumente GmbH, Germany) between the first and the second ionization chamber ensures precise positioning of the sample environments relative to the beam position. Between the second and third ionization chamber, a motorized holder for reference foils is installed.

The transmission XAS setup can be combined with advanced setups for complementary characterization techniques like X-ray diffraction and infrared spectroscopy. This

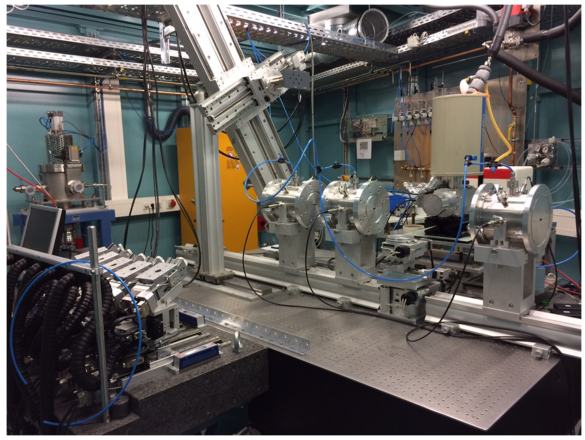

FIG. 6. Experimental setup for XAFS and XES measurements at the ACT station (experiment 1). The photo shows the high energy detection setup without He containments. See Sec. IV A for details.

allows to combine the information about the local molecular environment of catalytically active materials with the information related to the long range order structures and to study adsorbed reaction species simultaneously. XRD measurements in Debye-Scherrer geometry are realized using a MediPix area sensitive detector (University of Freiburg, Germany)[59] mounted on a motorized 2-axis stage (goniometer arm, HUBER Diffraktionstechnik, Rimsting, Germany) allowing to scan the scattering angle 2Θ from 0° to 90° and to adjust the sample to detector distance according to the actual requirements.

Another option is to combine XAS and DRIFTS measurements[60,61] using a VERTEX 70 spectrometer (Bruker AXS GmbH, Germany, switched to an external beam path), Harrick Praying Mantis mirror optics, and a specially designed transmission cell for powder samples.[62,63] The complete

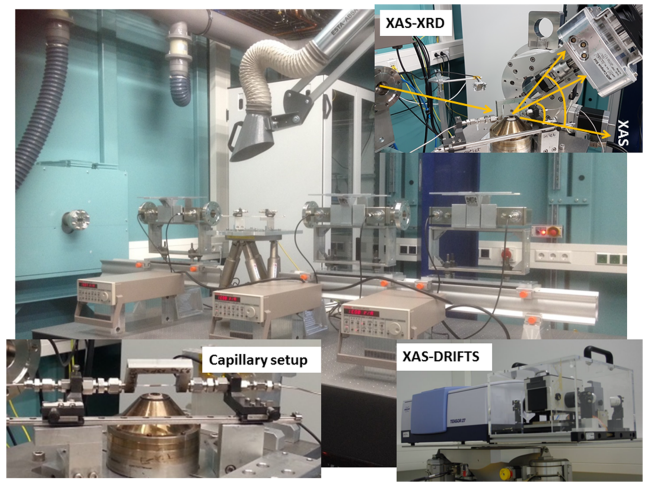

FIG. 7. Experimental setup for XAS measurements in transmission mode at the CAT station (experiment 2): 3 ionization chambers for simultaneous sample and reference sample measurements (OKEN Ltd.), Keithley K428 electrometers, flexible chemical exhaust, PI heavy load hexapod for alignment of the sample relative to the beam position with the continuous flow capillary as an *in situ* cell. Insets: capillary setup with the gas blower (left), combined XAS-XRD setup (top, right), and XAS-DRIFTS setup (bottom, right). See Sec. IV B for details.

DRIFTS setup is mounted on a custom-made 5-axis (tripod and rotations) stage (HUBER Diffraktionstechnik, Rimsting, Germany) between the first and second ionization chamber instead of the hexapod and can be aligned relative to the monochromatic X-ray beam. This setup allows simultaneous XAS and DRIFTS measurements providing valuable complementary information, e.g., about the catalyst structure and adsorbed species.

V. INFRASTRUCTURE AND PROTOCOL FOR HANDLING RADIOACTIVE SAMPLES

Since 2004, ANKA holds a license to handle non-fissile radioactive isotopes with activities up to 10^6 times the (isotope specific) European exemption limit,[64] regardless of the decay channel, and 10^5 times the exemption limit for 231-Pa inside the INE-Beamline experimental hutch. This license was extended in 2011 to include as well 200 mg each of the fissile isotopes 235-U and 239-Pu. In the case of the simultaneous presence of several radionuclides in a set of samples, a simple sum rule has to be applied, i.e., the summed percentages from the maximum allowed amounts for each nuclide have to stay below 100%. With commissioning of the ACT laboratory, the amounts covered by this license have been doubled to allow for the same isotopes and sample activities present at both laboratories (ACT and INE-Beamline) during coinciding experiments. The rounded activity values for exemption limits generally range between 10^3 Bq for most α-emitting actinides and 10^9 Bq for low energy β-emitters (e.g., 3-H). To give an example, for the actinide nuclides 243-Am and 242-Pu, the total mass allowed to be studied at the ACT experimental station would be 140 mg and 66 g, respectively.

To offer sufficient flexibility for X-ray spectroscopy investigations, while at the same time enforcing KIT and ANKA radiation safety precautions, a protocol for work at the ACT laboratory in the presence of radioactivity has been implemented. The protocol adheres to procedures successfully applied and supervised for more than a decade by INE radiation safety officers supported by KIT radiation protection technicians (as outlined in Ref. 17). All radioactive samples measured at the ACT station must be enclosed within two independent protective layers or containments. Generally, sealed polyethylene tubes, vials, or bags are the first containment, and specific sample cells, also inert gas flushed cells preventing oxygen or moisture sensitive samples from air contact, serve as the second containment. This double containment concept ensures versatility by avoiding the need for installation of a glove box in the experimental hutch, which facilitates accommodation of different sample geometries, e.g., for studies at low photon energies. Samples for investigation at the ACT station are either directly prepared at INE's controlled area radioactive laboratories or shipped to INE for inspection and integrity checks. Transports between INE labs and the ACT and INE-Beamline stations are classified as internal transports and are therefore fast and require a minimum of administrative effort. The entire procedure of removing a sample cell from an inert gas glove-box in the INE controlled area labs, screening for outer contamination by radiation protection personnel, packing, transport, unpacking, rescreening, and starting data acquisition at the beamline can be completed within 20 min. Since the samples are also retrievable, sample characterization in INE laboratories with the available instrumentation shortly following the experiments at the beamlines and back-transport is possible. Exchange of radioactive samples between both experimental stations (ACT and INE-Beamline) is possible without prior back-transport to INE. The infrastructure for radioactive experiments at the ACT station includes an independent ventilation system producing about 20 Pa negative-pressure in the experimental hutch and exhausting to the ANKA hall exterior through high-efficiency particulate air (HEPA) filters, a hand-foot contamination monitor and hand-held monitor provided in the INE-Beamline personnel lock, video surveillance inside the experimental hutch and lock room, and a fire resistant cabinet for sample storage when samples are not being measured such as during inadvertent interruption of ANKA operation. Fully automated and unattended data acquisition, e.g., during overnight runs, is permitted for experiments deemed safe, with radiation safety officers on call.

VI. INFRASTRUCTURE FOR CATALYTIC *IN SITU* AND *OPERANDO* STUDIES

The CAT experimental station operated by KIT-ITCP and KIT-IKFT is equipped with a special infrastructure for *in situ* and *operando* catalytic studies, including stationary reactive gas supply, precise gas dosing systems, and on-line product analysis.

The on-site reactive gas infrastructure includes two fireproof ventilated gas bottle cabinets (European standard EN 14470-2) outside the experimental hutch, gas transfer lines to gas manifolds inside the experimental hutch, and an automatic gas warning system along with an independent ventilation and a chemical exhaust system ensuring that personnel and equipment are protected from harmful, toxic, flammable, or corrosive gas exposure according to the safety regulations of ANKA and KIT. The system is designed to supply all gases listed in Table IV.

The reactive gas is delivered to gas dosing units equipped with mass flow controllers (Bronkhorst High-Tech B.V., Germany) ensuring precise dosing and stable flow rates in the following conduit and distribution system (B.E.S.T. Fluidsysteme GmbH, Swagelok Stuttgart, Germany) and sample cells. The available mass flow controllers are specified for gases listed in Table IV and maximum flow rates of 5 ml/min or 100 ml/min. A mass spectrometer (ThermoStar™ GSD 320 T1, 1-100 amu, Iridium filament, heated capillary 200 °C, Pfeiffer Vacuum GmbH, Germany) for detection and quantification of reaction products can be connected to the outlet of the sample cells and can detect most of the common products down to 100 ppb.

A number of specially designed and approved sample environments for catalytic experiments under realistic reaction conditions in gas phase, at high pressure, at elevated temperature, or in liquid phase are available. The workhorse for catalytic studies is a continuous flow quartz capillary cell for powder samples[21,37] at temperatures up to 900 °C, heated by a gas blower (FMB Oxford, UK) mounted directly under

TABLE IV. Reactive gas supply for *in situ*/*operando* studies at the CAT experimental station.

Line	System	Gas	Volume/concentration
1	High pressure H_2	Pure H_2 (max. 200 bars)	2-50 l/100%
2	High pressure CO_2/CO	Liquid CO_2 (max. 50 bars)	2-10 l/100%
		CO max. (max. 200bar)	2-10 l/100%
3	Normal pressure H_2	Pure H_2	10-50 l/100%
		H_2 containing test gases (diluted in He)	2-10 l/5%-25%
4	Flammable and toxic test gases (diluted in He)	CO/He or Ar	2-10 l/100 ppm–5%
		CO_2/He	2-10 l/100 ppm–10%
		C_xH_y test gases (diluted in He)	2-10 l/5%
5	Flammable test gases	C_xH_y	2-10 l/5%
		NH_3	2-10 l/100 ppm up to 1%
6	NOx containing test gases	NO/He	2-10 l/5%
		NO_2/He	2-10 l/5%
7	Sulfur containing gases	H_2S, SO_x	2-10 l
8	Oxygen containing gases	Air/O_2	10-50 l/2%-100% O_2

the capillary. The catalyst bed is placed inside the capillary, which is in turn connected to the gas supply and analysis system described above. The complete capillary setup including the gas blower is mounted on the hexapod in such a way that the sample can be aligned relative to the monochromatic X-ray beam without breaking the gas atmosphere or interrupting the reaction.

Further examples are setups for studying colloidal synthesis of nanoparticles[65] and for reactions at high pressure (up to 150 bars[66,67]). The *in situ* and *operando* setups installed at the CAT experimental station are of flexible design, so that users can bring their own reaction cells and gas mixing systems and integrate them into the existing infrastructure if necessary.

VII. RESEARCH EXAMPLES

Pilot XAS experiments with samples relevant for both scientific fields were successfully carried out during the initial beamline commissioning phase at the end of 2015.[68] Sections VII A–VII C present further details on initial and ongoing studies conducted since then at both experimental stations.

A. ACT: Determination of uranium bonding characteristics in $Rb_2UO_2Cl_4$ by U M_4-edge HR-XANES spectroscopy

Uranium (U) is the major constituent of most HAW matrices. An important aspect in the assessment of the long-term safety and evolution of a projected nuclear waste repository is to understand the physical and chemical properties of U and radiotoxic *trans*-uranium elements (Np, Pu, Am, Cm) which are generated in nuclear fission reactors. The environmental reactivity of An elements is largely determined by their physicochemical state or speciation, encompassing valence or oxidation state and molecular coordination sphere of the complexed metal cations. The formation of linear *trans*-dioxo or "actinyl" cations (O = An = O^{n+}, n = 1,2) with strong axial oxygen bonds and weak bonds to equatorial ligands is characteristic for the early actinides U–Pu in their penta- or hexavalent oxidation state. High energy resolution X-ray absorption near edge structure (HR-XANES) in the tender X-ray regime covering the early An $M_{5,4}$-edges (3.3–4.0 keV) and An 3d4f resonant inelastic X-ray scattering (RIXS) are now available as bulk sensitive techniques directly probing electronic states and bonding characteristics in these systems with hitherto unseen precision.[56] Here we present an example from a recent master thesis project at KIT-INE,[69] where the influence of equatorial halide ligands on the U–O bond covalence and U 5f density of states in the uranyl moiety of $Rb_2UO_2X_4$ (X = Br, Cl, F)[70] was probed by U M_4 HR-XANES.

The samples were investigated at the ACT station with the beamline optics tuned to deliver a primary beam of about 1×1 mm^2 spot size on the sample in the vicinity of the U M_4-edge (~5.0×10^9 photons/s). U M_4-edge HR-XANES spectra of the UO_2 reference and $Rb_2UO_2X_4$ samples were recorded employing the multi-analyzer crystal X-ray emission spectrometer described in Sec. IV A. The DCM (Si ⟨111⟩ crystal pair) was calibrated by assigning 3725.2 eV to the maximum of the most intense absorption resonance (white line, WL) of the UO_2 U M_4 HR-XANES spectrum. The gas tight containment enclosing the spectrometer ensured a constant He atmosphere (<0.2% air content) during all measurements. Spectra were obtained by recording the maximum intensity of the U M_β emission line (3339.8 eV)—diffracted by the five spherically bent Si(220) crystal analyzers (Saint-Gobain Crystals, France) and focused onto a single diode VITUS silicon drift detector (VITUS SDD KETEK, Munich, Germany)—as a function of the incident photon energy. The crystals were aligned at a 75.17° Bragg angle. The HR-XANES spectra were recorded with two different experimental energy resolutions, which are denoted as "low" and "high." To achieve high resolution, the beam size was confined to 500×500 μm size by aligning a four blade slit in front of the sample. Spectra were recorded with 0.1 and 0.5 eV step size at the edge and post-edge regions, respectively, and an integration time of 2 s/step. Typically, two scans were collected at room temperature and averaged. All spectra were normalized to their edge jump. $Rb_2UO_2X_4$ crystals were measured as finely ground powders spread on a

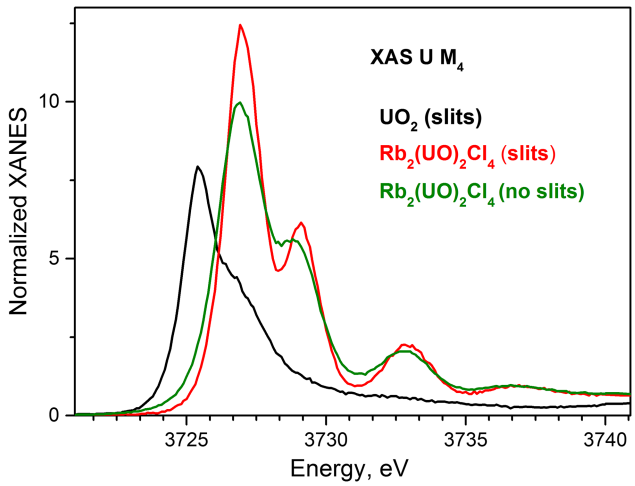

FIG. 8. U M4 HR-XANES of $Rb_2UO_2Cl_4$ measured at low and high resolution in comparison to the UO_2 reference sample.

double sided adhesive tape and fixed inside a Plexiglas holder adhering to the double containment rule with 8 and 13 μm KAPTON® film windows for inner and outer containments, respectively.

As an example, Fig. 8 depicts the U M_4 HR-XANES of $Rb_2UO_2Cl_4$ measured at low and high resolution in comparison to the UO_2 reference. The edge sharpening effect of the additional slit is clearly visible. The experimental energy resolution in the high resolution mode amounts to 1.2 eV and is close to the 0.9 eV calculated experimental energy resolution—encompassing broadening due to the large beam spot size and limited DCM and HRXES spectrometer resolution.[71] The WL positions of the U M_4 HR-XANES spectra are observed to shift toward higher energies within the Br, Cl, and F series (not shown), which is in agreement with the calculated increase of the partial positive charge at the U center derived from a Mulliken population analysis. Surprisingly, this increase is not a direct but an indirect consequence of the increasing electronegativity of the halogen ligand. Whereas the partial charge is almost the same for the three halide anions, the negative partial charge of oxygen increases when exchanging Br by Cl and Cl by F, which in turn reflects an increase of ionic bond character of the U–O bond in this order.[69]

B. CAT: *In situ* study of Ni/Fe catalysts during temperature programmed reduction

Research at ITCP and IKFT is focused on catalysts for energy related applications (synthetic fuels, conversion of biomass platform molecules), selective oxidation, sustainable fine chemical processes, and exhaust gas after treatment.

One of the challenges for a sustainable future electrical power supply based on renewable energy (like wind and sunlight) concerns its long-term storage to balance its fluctuating availability.[34,72,73] One of the promising chemical energy carriers is methane, which can be produced within the "Power-to-Gas" concept.[74] Renewable H_2 produced by water electrolysis with excess electrical power from renewable sources is used to hydrogenate the greenhouse gas CO_2 to synthetic natural gas.[75,76] Methane can be stored and distributed in the existing natural gas grid, which is one of the major advantages compared to H_2 as an energy storage compound. Nickel is the most widely used catalyst due to its high activity and low cost.[77–81] The influence of the crystalline and electronic structure of Ni particles on the performance of Ni-based catalysts is still a matter of investigation.[82,83] It was found that during abrupt load changes rapid phase transformations and deactivation of the Ni particles occur.

One approach for a rational catalyst design with the goal to enhance the activity of Ni-based catalysts is alloying nickel with other metals, such as iron or rhodium. Ni/Fe alloy catalysts are known to increase the dissociation of the C–O bond during methanation reactions,[84–86] whereas noble metal promotion enhances the reducibility and stability of the Ni-based catalyst.[87–89] The *in situ* XAS study of a 17 wt. % Ni_3Fe/γ-Al_2O_3 catalyst synthesized by Mutz and Serrer[90,91] was carried out to clarify the structure of the bimetallic material and its behavior during temperature programmed reduction (TPR) in 50% H_2/He (total flow 50 ml/min, 10 K/min rate). Measurements were performed using the continuous flow capillary setup containing an approximately 10 mm long packed bed of the Ni_3Fe/γ-Al_2O_3 catalyst diluted with γ-Al_2O_3 (100–200 μm sieve fraction) heated by the air gas blower.[21,37] The XAS data were recorded at both Ni K (8333 keV) and Fe K (7112 keV) absorption edges in transmission mode and analyzed using the IFEFFIT package.[92] The normalized XANES spectra of the catalyst during TPR are shown in Fig. 9 (left). The changes in the spectral shape of both Ni K and Fe K XANES can be attributed to the reduction of the metal particles after heating in H_2 flow. Detailed analysis of the spectra using the linear combination fitting module of Athena showed that the iron oxide is quickly reduced to FeO at about 200 °C before significant reduction of nickel, starting at circa 320 °C. In the end of the TPR, the sample was kept at 500 °C in 50% H_2/He atmosphere for about 1 h. The "activated" Ni_3Fe particles contained about 80% metallic Ni, 20% NiO, 60% metallic Fe, 25% FeO, and 15% γ-Fe_2O_3 (Fig. 9, right).

Normalized Ni K and Fe K XANES spectra of the Ni_3Fe/γ-Al_2O_3 catalyst before and after the TPR at room temperature together with the corresponding spectra of reference materials are shown in Fig. 10 (left). The electronic structure of the Ni and Fe atoms in their initial state is rather close to NiO and γ-Fe_2O_3, respectively. After the TPR, the XANES spectra of Ni and Fe differ significantly compared to the initial state and featured Ni and Fe in a reduced state. Ni K EXAFS $k^3\chi(k)$ data of the Ni_3Fe/γ-Al_2O_3 catalyst and its Fourier transform before and after the TPR at room temperature are plotted in Fig. 10 (right) together with the data for Ni and NiO reference materials. The quality of the EXAFS signal up to k = 14 $Å^{-1}$ allows us to draw conclusions about the preservation of the local atomic surrounding of Ni atoms in both oxidized and reduced states with a decreasing second shell coordination number and a decrease in the long range order compared to the bulk materials. These *in situ* studies provide information about the structure of the bimetallic catalyst and indicate the presence of small, slightly modified particles compared to the bulk material. Ni/Fe particles in the activated state are found to be still partially oxidized at both atomic sites. Based on this knowledge, the behavior

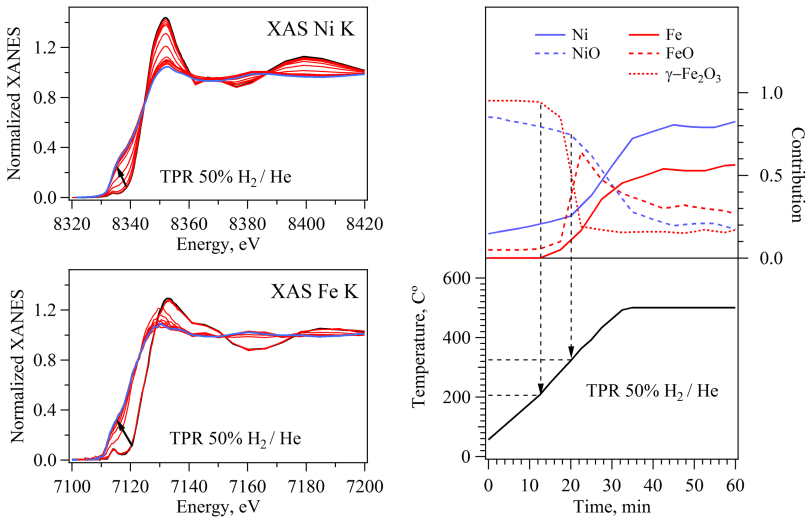

FIG. 9. (Left) Normalized Ni K and Fe K XANES spectra of a $Ni_3Fe/\gamma\text{-}Al_2O_3$ catalyst during TPR. Arrows show changes in the absorption behavior with time. (Right) Temperature and contributions of different oxidation states of Ni and Fe during TPR.

of the catalyst under dynamically changing conditions will be further studied by *operando* XAS combined with XRD at CAT-ACT.

C. CAT: *Operando* study of a bifunctional catalyst for one-step DME synthesis at elevated pressure

Dimethyl ether (DME) is a valuable platform chemical which recently has been considered as a potential clean and sustainable fuel for diesel (compression-ignition) engines.[93] Traditionally, DME is produced by dehydration of methanol, which is obtained from syngas over Cu-based catalysts. An innovative one-step DME synthesis from the syngas allowing higher CO conversion can be achieved over bifunctional catalysts based on metal nanoparticles supported on acidic carriers.[94] Alternative catalysts for the DME production need to be found as Cu catalysts used for methanol synthesis are prone to deactivation, mainly due to oxidation and/or sintering of Cu species.[95–97]

Operando XAS on a state-of-the-art $Cu/ZnO/\gamma\text{-}Al_2O_3$ DME catalyst (synthesized by Behrens group at KIT-IKFT)[94] was carried out to set a benchmark for potential studies of novel catalyst formulations at elevated pressure. XANES and EXAFS data were recorded at the Cu K and Zn K absorption edges in order to derive structure-activity relationships during reductive activation and DME synthesis. Acquisition of one XANES spectrum took about 7 min at Cu K and Zn K edges, which were measured sequentially; during this period, the temperature increases by about 14 °C. The experiment was performed in a 1.5 mm quartz capillary used as *in situ* catalytic microreactor on calcined, pressed, and sieved catalyst powder (sieve fraction 100–200 μm). The catalyst containing 12.5 wt. % Cu and 28.4 wt. % Zn was further diluted with $\gamma\text{-}Al_2O_3$ (1:3 by weight) before granulating and sieving. First, the catalyst was exposed to 5%H_2/He (total flow 50 ml/min) during reductive activation (temperature ramp up to 250 °C, 1 °C/min ramp rate). Afterwards, the catalyst was exposed to a syngas mixture (15% CO + 15% H_2/He) at an elevated pressure of 15

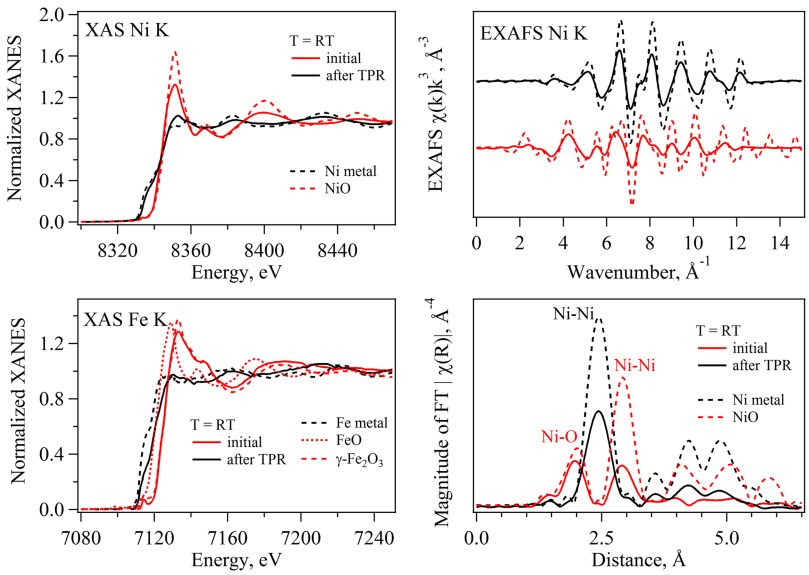

FIG. 10. (Left) Normalized Ni K and Fe K XANES spectra of a $Ni_3Fe/\gamma\text{-}Al_2O_3$ catalyst before and after TPR at room temperature together with the corresponding spectra of reference materials. (Right) The Ni K EXAFS $\chi(k)k^3$ signal and its Fourier transform (phase corrected) of the $Ni_3Fe/\gamma\text{-}Al_2O_3$ catalyst before and after TPR at room temperature together with data for Ni and NiO reference materials.

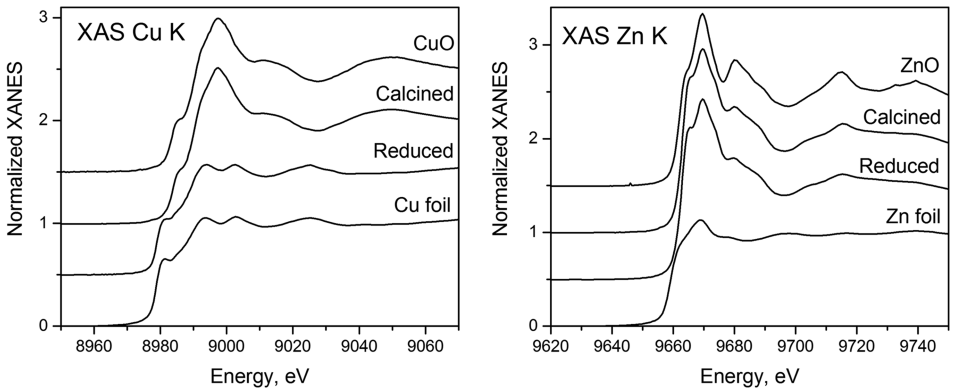

FIG. 11. XANES spectra recorded at (left) Cu K and (right) Zn K edges of the Cu/ZnO/γ-Al_2O_3 catalyst after calcination (as-received) and after reductive activation (in 5% H_2/He, 250 °C) as well as the corresponding reference spectra.

bars. The pressure was kept at 15 bars for 14 min after which the system was depressurized to 3.2 bars and kept for 60 min before recording XAS spectra. XAS data at both absorption edges were recorded during both reduction (*in situ*) and DME synthesis (*operando*) and were processed using the IFFEFIT software package.[92] The outlet gas composition was analyzed using the mass spectrometer.

Figure 11 shows Cu K and Zn K XANES spectra of the as-received (calcined) Cu/ZnO/γ-Al_2O_3 catalyst and the same catalyst after the reductive activation together with XANES spectra of the corresponding reference materials. In the as-received catalyst, both Cu and Zn were found to be oxidized in form of CuO and ZnO. During the reductive activation, CuO underwent a fast reduction to CuO in the temperature range from 120 °C to 135 °C without any significant intermediate Cu^+ formation, while Zn did not change its oxidation state. The change in the XANES spectra at the Cu K edge (Fig. 12) confirmed full reduction of CuO to metallic Cu nanoparticles, supported by the EXAFS results. The change in the EXAFS spectra at the Zn K edge (not shown here) suggested some decrease in the ZnO particle size resulting from the reductive pretreatment. High pressure DME synthesis conditions resulted in a small increase in Cu–Cu backscattering intensity (peak at 2.54 Å) (Fig. 11) without any signs of re-oxidation. The analysis of the EXAFS data reveals some sintering of Cu nanoparticles while no signs of Cu oxidation could be observed. Recently, other bimetallic catalysts were successfully characterized at 1 and 20 bars. The results of these experiments provide a novel insight into structure-performance relationships of these materials for DME synthesis and will be reported in a forthcoming publication.[98]

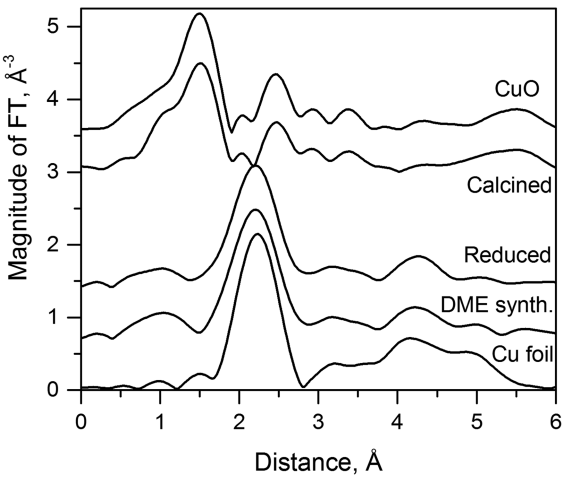

FIG. 12. Fourier transforms (in the *k*-range 3-11 $Å^{-1}$) of k^2-weighted EXAFS spectra recorded at the Cu K edge of the Cu/ZnO/γ-Al_2O_3 catalyst after calcination, after reductive activation (in 5% H_2/He, 250 °C), and during high pressure DME synthesis along with the corresponding reference spectra.

VIII. OUTLOOK—THE FUTURE OF CATALYSIS AND ACTINIDE SCIENCE AT ANKA

After successful commissioning and initial feasibility studies, future activities driven by CAT-ACT will strongly focus on research needs in the fields of actinide and catalysis research, e.g., of the exhaust gas lab Karlsruhe, the involved Helmholtz programs "Renewable Energies" (EE), "Science and Technology of Nanosystems" (STN), "Storage and Cross-linked Infrastructures" (SCI), "From Matter to Materials and Life" (MML), and "Nuclear Waste Management and Safety" (NUSAFE)—or research in the frame of "BMBF Verbundforschung" (Federal Ministry of Education and Research network program). It is obvious that these activities cover to a large extend questions pivotal in addressing environmental catalysis and the German "Energiewende" or energy transition strategy—i.e., the restructuring of electricity generation, distribution, and storage systems from those previously based on large scale power plant facilities to renewable, decentralized sources. This is only one of the future topics that require an integrated catalysis infrastructure with reactive gas atmosphere at elevated pressure and where real catalytic experiments are performed directly at the synchrotron radiation source and which may also be a seed for advanced infrastructure at other synchrotron radiation sources in future. Solving the nuclear waste disposal safety case is an integral part of this unprecedented effort.

As future beamline upgrades, implementation of further spectroscopic setups for correlative spectroscopies, a Quick-EXAFS mode requiring an additional fast DCM, a micro-focus option based on a Kirkpatrick-Baez mirror system, and the upgrade of the available detector pool encompassing new multi-element solid state detectors and a large area CCD detector for diffraction measurements [including high energy X-ray scattering (HEXS)/PDF measurements] are envisaged.

Additionally, development of innovative *in situ* cells for radionuclide and catalysis research is a major part of future instrumental upgrading. The infrastructure for catalysis research will be complemented by an off-line catalysis lab adjacent to the experimental floor, offering sample preparation and pre- and post-characterization capabilities including kinetic studies.

Apart from the in-house research activities under the auspices of KIT institutes ITCP, IKFT, and INE, access to the CAT-ACT beamline and its auxiliary lab infrastructure is offered to external cooperation partners from the academia on the basis of common research projects or as a commercial service.

ACKNOWLEDGMENTS

The authors thank KIT, ANKA, BMBF (within the project "Materials in Action"), HGF programs Renewable Energies (EE), Science and Technology of Nanosystems (STN), Storage and Cross-linked Infrastructures (SCI), from Matter to Materials and Life (MML), Nuclear Waste Management and Safety (NUSAFE) and the European Commission Joint Research Centre, Directorate for Nuclear Safety and Security (Karlsruhe) for financial support. T. Vitova received funding through the Helmholtz Young Investigator Group VH-NG-734. Wolfgang Mexner (KIT), David Haas (KIT), Denis Jakel (KIT), and David Cemin (KIT) are acknowledged for valuable contributions to the design of the beamline control system and support during component factory acceptance tests. Finally, we thank the following people for their input for the scientific examples in this paper: Silke Behrens, Manuel Gentzen, Benjamin Mutz, and Marc-André Serrer (all KIT).

[1] Y. Iwasawa, K. Asakura, and M. Tada, *XAFS Techniques for Catalysts, Nanomaterials, and Surfaces* (Springer International Publishing, 2017).
[2] D. C. Koningsberger and R. Prins, *X-Ray Absorption: Principles, Applications, Techniques of EXAFS, SEXAFS and XANES* (Wiley-VCH Verlag GmbH & Co., 1987).
[3] S. Thierfeldt and F. Schartmann, *Stilllegung und Rückbau Kerntechnischer Anlagen–Erfahrungen und Perspektiven* (Brenk Systemplanung, Aachen, Germany, 2012).
[4] U. Heinen-Esser and M. Müller, *Verantwortung für die Zukunft–Ein Faires und Transparentes Verfahren für die Auswahl eines Nationalen Endlagerstandortes (Abschlussbericht)* (Kommission Lagerung Hoch Radioaktiver Abfallstoffe, Berlin, Germany, 2016).
[5] M. A. Denecke, in *X-Ray Absorption and X-Ray Emission Spectroscopy*, edited by J. A. van Bokhoven (Wiley & Sons, Chichester, United Kingdom, 2016), Vol. 2, pp. 523–560.
[6] M. A. Denecke, Coordin. Chem. Rev. **250**(7-8), 730 (2006).
[7] K. Dardenne, E. González-Robles, J. Rothe, N. Müller, G. Christill, D. Lemmer, R. Praetorius, B. Kienzler, V. Metz, G. Roth, and H. Geckeis, J. Nucl. Mater. **460**, 209 (2015).
[8] E. Curti, A. Froideval-Zumbiehl, I. Gunther-Leopold, M. Martin, A. Bullemer, H. Linder, C. N. Borca, and D. Grolimund, J. Nucl. Mater. **453**(1-3), 98 (2014).
[9] C. Degueldre, S. Pin, J. Poonoosamy, and D. A. Kulik, J. Phys. Chem. Solids **75**(3), 358 (2014).
[10] K. O. Kvashnina, Y. O. Kvashnin, and S. M. Butorin, J. Electron Spectrosc. Relat. Phenom. **194**, 27 (2014).
[11] I. Pidchenko, K. O. Kvashnina, T. Yokosawa, N. Finck, S. Bahl, D. Schild, R. Polly, E. Bohnert, A. Rossberg, J. Gottlicher, K. Dardenne, J. Rothe, T. Schafer, H. Geckeis, and T. Vitova, Environ. Sci. Technol. **51**(4), 2217 (2017).
[12] M. Plaschke, J. Rothe, M. K. Armbruster, M. A. Denecke, A. Naber, and H. Geckeis, J. Synchrotron Radiat. **17**, 158 (2010).
[13] T. Vitova, M. A. Denecke, J. Göttlicher, K. Jorissen, J. J. Kas, K. Kvashnina, T. Prüßmann, J. J. Rehr, and J. Rothe, J. Phys.: Conf. Ser. **430**, 012117 (2013).
[14] T. Vitova, J. C. Green, R. G. Denning, M. Löble, K. Kvashnina, J. Kas, K. Jorissen, J. Rehr, T. Malcherek, and M. A. Denecke, Inorg. Chem. **54**(1), 174 (2015).
[15] T. Vitova, K. O. Kvashnina, G. Nocton, G. Sukharina, M. A. Denecke, S. M. Butorin, M. Mazzanti, R. Caciuffo, A. Soldatov, T. Behrends, and H. Geckeis, Phys. Rev. B **82**, 23 (2010).
[16] W. Matz, N. Schell, G. Bernhard, F. Prokert, T. Reich, J. Claussner, W. Oehme, R. Schlenk, S. Dienel, H. Funke, F. Eichhorn, M. Betzl, D. Prohl, U. Strauch, G. Huttig, H. Krug, W. Neumann, V. Brendler, P. Reichel, M. A. Denecke, and H. Nitsche, J. Synchrotron Radiat. **6**(6), 1076 (1999).
[17] J. Rothe, S. Butorin, K. Dardenne, M. A. Denecke, B. Kienzler, M. Loble, V. Metz, A. Seibert, M. Steppert, T. Vitova, C. Walther, and H. Geckeis, Rev. Sci. Instrum. **83**(4), 043105 (2012).
[18] C. N. Borca, D. Grolimund, M. Willimann, B. Meyer, K. Jefimovs, J. Vila-Comamala, and C. David, J. Phys.: Conf. Ser. **186**(1), 012003 (2009).
[19] I. L. Lorens, P. L. Solari, B. Sitaud, R. Bes, S. Cammelli, H. Hermange, G. Othmane, S. Safi, P. Moisy, S. Wahu, C. Bresson, L. Schlegel Michel, D. Menut, J.-L. Bechade, P. Martin, J.-L. Hazemann, O. Proux, and C. Den Auwer, Radiochim. Acta **102**, 957 (2014).
[20] S. R. Bare and T. Ressler, Adv. Catal. **52**, 339 (2009).
[21] J.-D. Grunwaldt, M. Caravati, S. Hannemann, and A. Baiker, Phys. Chem. Chem. Phys. **6**(11), 3037 (2004).
[22] J.-D. Grunwaldt and B. S. Clausen, Top. Catal. **18**(1-2), 37 (2002).
[23] J.-D. Grunwaldt and A. I. Frenkel, Synchrotron Radiat. News **22**(1), 2 (2009).
[24] H. Topsøe, J. Catal. **216**(1–2), 155 (2003).
[25] B. M. Weckhuysen, Phys. Chem. Chem. Phys. **5**(20), 4351 (2003).
[26] T. Günter, D. E. Doronkin, H. W. P. Carvalho, M. Casapu, and J.-D. Grunwaldt, J. Phys.: Conf. Ser. **712**(1), 012071 (2016).
[27] O. Deutschmann and J.-D. Grunwaldt, Chem. Ing. Tech. **85**(5), 595 (2013).
[28] M. Votsmeier, T. Kreuzer, J. Gieshoff, and G. Lepperhoff, *Automobile Exhaust Control* (Wiley-VCH Verlag GmbH & Co., 2012).
[29] T. Lunkenbein, J. Schumann, M. Behrens, R. Schlogl, and M. G. Willinger, Angew. Chem., Int. Ed. **54**(15), 4544 (2015).
[30] J.-D. Grunwaldt, A. M. Molenbroek, N. Y. Topsoe, H. Topsoe, and B. S. Clausen, J. Catal. **194**(2), 452 (2000).
[31] B. H. Davis and M. L. Occelli, *Fischer-Tropsch Synthesis, Catalysts, and Catalysis: Advances and Applications* (CRC Press, 2016).
[32] N. Dahmen, E. Dinjus, T. Kolb, U. Arnold, H. Leibold, and R. Stahl, Environ. Prog. Sustainable Energy **31**(2), 176 (2012).
[33] J.-D. Grunwaldt, *Chemical Energy Storage* (Walter de Gruyter, Berlin/Boston, 2013).
[34] K. F. Kalz, R. Kraehnert, M. Dvoyashkin, R. Dittmeyer, R. Glaser, U. Krewer, K. Reuter, and J. D. Grunwaldt, ChemCatChem **9**(1), 17 (2017).
[35] Y. Iwasawa, *X-Ray Absorption Fine Structure for Catalysts and Surfaces* (World Scientific Publishing Co Pte Ltd., Singapore, Singapore, 1996).
[36] J.-D. Grunwaldt and A. Baiker, Catal. Lett. **99**(1-2), 5 (2005).
[37] J.-D. Grunwaldt, N. van Vegten, and A. Baiker, Chem. Commun. **44**, 4635 (2007).
[38] D. Ciuparu, M. R. Lyubovsky, E. Altman, L. D. Pfefferle, and A. Datye, Catal. Rev. **44**(4), 593 (2002).
[39] B. S. Clausen, J. Schiotz, L. Grabaek, C. V. Ovesen, K. W. Jacobsen, J. K. Norskov, and H. Topsoe, Top. Catal. **1**(3-4), 367 (1994).
[40] M. Hagelstein, A. San Miguel, A. Fontaine, and J. Goulon, J. Phys. IV **7**(C2), 303 (1997).
[41] See http://www.esrf.eu/UsersAndScience/Experiments/CRG/BM01/bm01b for information about BM01 beamline at ESRF; accessed 24 November 2017.
[42] V. Briois, C. L. Fontaine, S. Belin, L. Barthe, Th. Moreno, V. Pinty, A. Carcy, R. Girardot, and E. Fonda, J. Phys.: Conf. Ser. **712**(1), 012149 (2016).
[43] See https://www.anka.kit.edu/992.php for information about XAS beamline at KIT synchrotron facility; accessed 24 November 2017.
[44] J.-D. Grunwaldt, S. Hannemann, J. Gottlicher, S. Mangold, M. A. Denecke, and A. Baiker, Phys. Scr. **T115**, 769 (2005).
[45] O. Muller, M. Nachtegaal, J. Just, D. Lutzenkirchen-Hecht, and R. Frahm, J. Synchrotron Radiat. **23**(1), 260 (2016).
[46] See https://petra3-extension.desy.de/e84814/e86688/ for information about P064 beamline at PETRA III; accessed 24 November 2017.
[47] See https://petra3-extension.desy.de/e84814/e86689/ for information about P065 beamlineat PETRA III; accessed 24 November 2017.

[48]K. Klementiev, K. Norén, S. Carlson, K. G. V. S. Clauss, and I. Persson, J. Phys.: Conf. Ser. **712**(1), 012023 (2016).
[49]See https://www.anka.kit.edu for information about KIT synchrotron facility; accessed 24 November 2017.
[50]See http://www.knmf.kit.edu for information about KNMF facility; accessed 24 November 2017.
[51]J. Stotzel, D. Lutzenkirchen-Hecht, and R. Frahm, Rev. Sci. Instrum. **81**(7), 073109 (2010).
[52]W. Mexner, K. H. Cerff, T. Spangenberg, and M. Hagelstein, presented at the PCaPAC 2008-International Workshop on Personal Computers and Particle Accelerator Controls, 2008.
[53]J. M. Chaize and A. Götz, presented at the PCaPAC 2005–Proceedings of the 5th International Workshop on Personal Computers and Particle Accelerator Controls, 2005.
[54]E. Kleymenov, J. A. van Bokhoven, C. David, P. Glatzel, M. Janousch, R. Alonso-Mori, M. Studer, M. Willimann, A. Bergamaschi, B. Henrich, and M. Nachtegaal, Rev. Sci. Instrum. **82**(6), 065107 (2011).
[55]T. Pruessmann, "Characterization of bonding differences by advanced synchrotron based x-ray spectroscopy," Ph.D. thesis, Karlsruhe Institute of Technology (KIT), 2016.
[56]T. Vitova, I. Pidchenko, D. Fellhauer, P. S. Bagus, Y. Joly, T. Pruessmann, S. Bahl, E. Gonzalez-Robles, J. Rothe, M. Altmaier, M. A. Denecke, and H. Geckeis, Nat. Commun. **8**, 16053 (2017).
[57]D. Hudry, C. Apostolidis, O. Walter, A. Janssen, D. Manara, J. C. Griveau, E. Colineau, T. Vitova, T. Pruessmann, D. Wang, C. Kubel, and D. Meyer, Chem.-Eur. J. **20**(33), 10431 (2014).
[58]S. Mangold, R. Steininger, and T. Spangenberg, J. Phys.: Conf. Ser. **430**(1), 012022 (2013).
[59]M. Fiederle, D. Greiffenberg, J. Idarraga, J. Jakubek, V. Kral, C. Lebel, C. Leroy, G. Lord, S. Pospisil, V. Sochor, and M. Suk, Nucl. Instrum. Methods Phys. Res., Sect. A **591**(1), 75 (2008).
[60]N. S. Marinkovic, Q. Wang, and A. I. Frenkel, J. Synchrotron Radiat. **18**, 447 (2011).
[61]M. A. Newton, B. Jyoti, A. J. Dent, S. G. Fiddy, and J. Evans, Chem. Commun. **2004**(21), 2382.
[62]A. M. Gänzler, H. Lichtenberg, A. I. Frenke, M. Casapu, A. Boubnov, D. Wang, and J.-D. Grunwaldt, J. Phys.: Conf. Ser. **712**, 012045 (2016).
[63]Y. Zhou, D. E. Doronkin, M. L. Chen, S. Q. Wei, and J.-D. Grunwaldt, ACS Catal. **6**(11), 7799 (2016).
[64]*Radiation Protection 65, XI-028/93-en*, Report prepared by M. Harvey, S. Mobbs, J. Cooler, A. M. Chapius, A. Sugier, T. Schneider, J. Lochard, and A. Janssens (Commision of the European Communities, Luxembourg, 1993).
[65]G. Hofmann, G. Tofighi, G. Rinke, S. Baier, A. Ewinger, A. Urban, A. Wenka, S. Heideker, A. Jahn, R. Dittmeyer, and J.-D. Grunwaldt, J. Phys.: Conf. Ser. **712**, 012072 (2016).
[66]J.-D. Grunwaldt, M. Caravati, and A. Baiker, J. Phys. Chem. B **110**(20), 9916 (2006).
[67]J.-D. Grunwaldt, M. Ramin, M. Rohr, A. Michailovski, G. R. Patzke, and A. Baiker, Rev. Sci. Instrum. **76**(5), 054104 (2005).
[68]A. Zimina, K. Dardenne, M. A. Denecke, J.-D. Grunwaldt, E. Huttel, H. Lichtenberg, S. Mangold, T. Pruessmann, J. Rothe, R. Steininger, and T. Vitova, J. Phys.: Conf. Ser. **712**(1), 012019 (2016).
[69]A. Prokopchuk, "Preparation of $Rb_2UO_2X_4$ compounds (X=F, Cl, Br) and characterization of bonding differences by spectroscopy and quantum chemical methods," Batchelor thesis, Karlsruhe Institut of Technology, Karlsruhe, Germany, 2017.
[70]D. D. Schnaars and R. E. Wilson, Inorg. Chem. **52**(24), 14138 (2013).
[71]F. M. F. de Groot, M. H. Krisch, and J. Vogel, Phys. Rev. B **66**(19), 195113 (2002).
[72]R. Schlögl, *Chemical Energy Storage* (Walter de Gruyter GmbH, Berlin/Boston, 2013).
[73]F. Schüth, Chem. Ing. Tech. **83**(11), 1984 (2011).
[74]M. Sterner, *Bioenergy and Renewable Power Methane in Integrated 100% Renewable Energy Systems* (Kassel University Press GmbH, Kassel, Germany, 2009).
[75]G. Centi and S. Perathoner, Catal. Today **148**(3-4), 191 (2009).
[76]G. Centi and S. Perathoner, Greenhouse Gases: Sci. Technol. **1**(1), 21 (2011).
[77]W. Wang, S. Wang, X. Ma, and J. Gong, Chem. Soc. Rev. **40**(7), 3703 (2011).
[78]J. J. Gao, Q. Liu, F. N. Gu, B. Liu, Z. Y. Zhong, and F. B. Su, RSC Adv. **5**(29), 22759 (2015).
[79]S. Ronsch, J. Schneider, S. Matthischke, M. Schluter, M. Gotz, J. Lefebvre, P. Prabhakaran, and S. Bajohr, Fuel **166**, 276 (2016).
[80]S. Rahmani, M. Rezaei, and F. Meshkani, J. Ind. Eng. Chem. **20**(4), 1346 (2014).
[81]H. Muroyama, Y. Tsuda, T. Asakoshi, H. Masitah, T. Okanishi, T. Matsui, and K. Eguchi, J. Catal. **343**, 178 (2016).
[82]B. Mutz, H. W. P. Carvalho, W. Kleist, and J.-D. Grunwaldt, J. Phys.: Conf. Ser. **712**, 012050 (2016).
[83]B. Mutz, H. W. P. Carvalho, S. Mangold, W. Kleist, and J.-D. Grunwaldt, J. Catal. **327**, 48 (2015).
[84]M. Andersson, T. Bligaard, A. Kustov, K. Larsen, J. Greeley, T. Johannessen, C. Christensen, and J. Norskov, J. Catal. **239**(2), 501 (2006).
[85]J. Sehested, K. E. Larsen, A. L. Kustov, A. M. Frey, T. Johannessen, T. Bligaard, M. P. Andersson, J. K. Norskov, and C. H. Christensen, Top. Catal. **45**(1-4), 9 (2007).
[86]S. Hwang, U. G. Hong, J. Lee, J. H. Baik, D. J. Koh, H. Lim, and I. K. Song, Catal. Lett. **142**(7), 860 (2012).
[87]S. Tada, D. Minori, F. Otsuka, R. Kikuchi, K. Osada, K. Akiyama, and S. Satokawa, Fuel **129**, 219 (2014).
[88]F. Ocampo, B. Louis, L. Kiwi-Minsker, and A.-C. Roger, Appl. Catal., A **392**(1-2), 36 (2011).
[89]W. Zhen, B. Li, G. Lu, and J. Ma, RSC Adv. **4**(32), 16472 (2014).
[90]B. Mutz, "Methanation of CO_2: Insight into deactivation mechanisms and catalyst stability under dynamic reaction conditions," Ph.D. thesis, Karlsruhe Institute of Technology (KIT), 2017.
[91]B. Mutz, M. Belimov, W. Wang, P. Sprenger, M.-A. Serrer, D. Wang, P. Pfeifer, W. Kleist, and J.-D. Grunwaldt, ACS Catal. **7**, 6802 (2017).
[92]B. Ravel and M. Newville, J. Synchrotron Radiat. **12**, 537 (2005).
[93]M. Müller and U. Hübsch, *Dimethyl Ether* (Wiley-VCH, 2000).
[94]M. Gentzen, W. Habicht, D. E. Doronkin, J.-D. Grunwaldt, J. Sauer, and S. Behrens, Catal. Sci. Technol. **6**(4), 1054 (2016).
[95]M. V. Twigg, Top. Catal. **22**(3/4), 191 (2003).
[96]H. H. Kung, Catal. Today **11**(4), 443 (1992).
[97]M. B. Fichtl, D. Schlereth, N. Jacobsen, I. Kasatkin, J. Schumann, M. Behrens, R. Schlögl, and O. Hinrichsen, Appl. Catal., A **502**, 262 (2015).
[98]M. Gentzen, D. E. Doronkin, T. L. Sheppard, J.-D. Grunwaldt, J. Sauer, and S. Behrens, "Bifunctional model catalysts based on colloidal Cu/Zn nanoparticles for the direct conversion of synthesis gas to dimethyl ether and hydrocarbons" (unpublished).